minerals

MDPI

Article

Composite Geopolymers Based on Mechanically Activated Fly Ash Blended with $SrCO_3$ (Strontianite) and $BaCO_3$ (Witherite)

Alexander M. Kalinkin [1,*], Elena V. Kalinkina [1], Ekaterina A. Kruglyak [1], Vasilij V. Semushin [1], Mikhail V. Chislov [2] and Irina A. Zvereva [2]

[1] Tananaev Institute of Chemistry, Subdivision of the Federal Research Centre "Kola Science Centre of the Russian Academy of Sciences", Akademgorodok 26a, Apatity 184209, Murmansk Region, Russia; e.kalinkina@ksc.ru (E.V.K.); e.kruglyak@ksc.ru (E.A.K.); v.semushin@ksc.ru (V.V.S.)

[2] Centre for Thermogravimetric and Calorimetric Research, Saint Petersburg State University, Universitetskaya nab. 7/9, St. Petersburg 199034, Russia; mikhail.chislov@spbu.ru (M.V.C.); irina.zvereva@spbu.ru (I.A.Z.)

* Correspondence: a.kalinkin@ksc.ru

Abstract: In this study, geopolymers based on mechanically activated mixtures of fly ash (FA) with $SrCO_3$ (strontianite) and $BaCO_3$ (witherite) were synthesized. NaOH solution was used as an alkaline agent and curing was carried out under ambient conditions. XRD, FTIR spectroscopy, thermogravimetry, and SEM were used to study the geopolymerization process and microstructure. The product of geopolymerization of the milled (FA + $SrCO_3$) and (FA + $BaCO_3$) blends was X-ray amorphous N-A-S-H gel. The beneficial impact of mechanical activation on the compressive strength of geopolymers was most evident during the initial stages of the curing process. The strength of geopolymers based on the (FA + carbonate) blends after 7 d was either less than the corresponding strength of geopolymers based on the 100% FA or, within the measurement accuracy, equal to it. With increasing curing time, the strength development of geopolymers synthesized from (70% FA + 30% carbonate) blends exceeded the strength growth of geopolymers containing less carbonates; after curing for 180 d, these geopolymers showed the highest compressive strength (20–27 MPa). This trend was more pronounced for the geopolymers based on the (FA + $SrCO_3$) blends. The influence of $SrCO_3$ and $BaCO_3$ addition to the FA on the strength of composite geopolymers was explained by dilution and microfiller effects. The geopolymers based on the FA blended with $SrCO_3$ and $BaCO_3$ exhibit potential applications in immobilizing radioactive strontium and producing radiation shielding materials.

Keywords: fly ash; strontium carbonate; barium carbonate; mechanical activation; geopolymers

Citation: Kalinkin, A.M.; Kalinkina, E.V.; Kruglyak, E.A.; Semushin, V.V.; Chislov, M.V.; Zvereva, I.A. Composite Geopolymers Based on Mechanically Activated Fly Ash Blended with $SrCO_3$ (Strontianite) and $BaCO_3$ (Witherite). *Minerals* **2023**, *13*, 1493. https://doi.org/10.3390/min13121493

Academic Editor: Francisco Franco

Received: 21 October 2023
Revised: 15 November 2023
Accepted: 27 November 2023
Published: 28 November 2023

1. Introduction

In recent decades, there has been significant research into synthesizing geopolymer materials using coal fly ash (FA) and other man-made raw materials. The term "geopolymer" was coined by D. Davidovits in the 1970s to describe alkali-activated metakaolin, the dehydrated and calcined form of the clay mineral kaolinite [1]. Over time, it has come to encompass a variety of synthetic low-calcium aluminosilicate polymeric materials, constituting a subset of the broader category known as alkali-activated binders [2]. The utilization of FA and other industrial solid by-products for the production of geopolymers addresses a significant challenge in waste management by converting potentially hazardous industrial residues into safe and value-added materials. In addition, it contributes to the reduction of the carbon footprint associated with Portland cement production. Geopolymers display characteristics that are comparable to or even superior to those of conventional cement-based concrete. They demonstrate high compressive strength, remark-

able thermal resistance, stability under irradiation, and resistance to acid attack and seawater exposure. Owing to these properties, geopolymers find application not only within the construction industry but also in diverse fields such as refractories and fire-resistant materials, immobilization of heavy metals, and wastewater treatment [3–6]. Currently, there is a gradually growing interest in the development of geopolymer materials for nuclear waste immobilization and radiation shielding applications [7–15].

The geopolymerization process of low-calcium (class F) FA is similar to that of metakaolin. In a simplified representation, this process includes interrelated reactions occurring after mixing the raw material with an alkaline agent (NaOH solution or liquid glass): (1) breakdown and dissolution of the raw material; (2) formation of a supersaturated aluminosilicate solution; (3) gelation (formation of N-A-S-H gel); (4) restructuring of the gel; and (5) polymerization and solidification, leading to the formation of a three-dimensional aluminosilicate network [16,17].

The class F FA, a readily available material, is often used in geopolymerization. However, its reactivity in this process is limited. To enhance the reactivity of FA with respect to an alkaline agent, and thereby improve geopolymer performance, two approaches have been employed. Firstly, mechanical activation (MA) or milling the FA in mills. In this context, both terms, "MA" and "milling", denote the same process of mechanical treatment a solid raw material in a planetary mill. Researchers have extensively studied the impact of milling on FA reactivity and geopolymer strength, as evidenced by numerous studies [18–26]. Secondly, various Ca/Mg-containing additives have been introduced into the FA, including abundant and cost-effective carbonate minerals such as calcite ($CaCO_3$) and dolomite ($CaMg(CO_3)_2$). The positive effect of the addition of Ca/Mg carbonate minerals to FA to improve geopolymer performance can be explained by filler, dilution, and chemical effects [27]. Unreacted carbonate particles act as fillers, enhancing packing density and compressive strength in geopolymer materials (the filler effect). Blending aluminosilicate raw materials with carbonates increases the alkali reagent/aluminosilicate ratio, accelerating geopolymerization (the dilution effect). The chemical effect is the most complex and least studied one due to the complicated nature of geopolymerization reactions. This effect depends on the carbonate nature, alkali reagent characteristics, carbonate/aluminosilicate ratio, solid component surface area, and curing conditions. Particularly, the chemical effect is associated with the partial dissolution of Ca/Mg carbonates in an alkaline medium. In geopolymer systems, calcium takes precedence over magnesium, significantly contributing to increased strength. Specifically, calcite demonstrates superior effectiveness compared to dolomite in enhancing the properties of geopolymer systems [28].

In our previous research, to the best of our knowledge, we were the first to combine the beneficial impact of adding Ca/Mg carbonates to FA and that of MA [29–31]. The study demonstrated that incorporating up to 10% of calcite or dolomite into the low calcium FA, followed by MA, notably enhanced the compressive strength of geopolymers. Moreover, a synergistic effect of these two factors (mixing the FA with the carbonates and MA) was observed, and it was noticeably greater for calcite than that for dolomite [30]. Unlike calcite and dolomite, the inclusion of magnesite in the FA did not enhance the strength of the composite geopolymer [31]. The lack of strength improvement was likely due to magnesite's chemical composition, where magnesium predominates while calcium is nearly absent. However, in most blends containing 1%–10% magnesite, the strength either remained stable or decreased minimally compared to the geopolymers made solely from 100% FA. This phenomenon can possibly be attributed to filler and dilution effects. The geopolymers based on the (FA + magnesite) blends exhibit potential application in producing the fire protection materials with enhanced properties.

In continuation of our previous studies, the aim of this work was to investigate the effect of including other alkaline earth metal carbonates, $SrCO_3$ (strontianite) and $BaCO_3$ (witherite), in the same FA following the same experimental procedure [29–31]. Geopolymers, as mentioned earlier, find applications in immobilizing nuclear waste, including

compounds containing radioactive strontium. It was revealed that during geopolymerization, soluble or sparingly soluble strontium salts tended to transform into $SrCO_3$ through atmospheric carbonation [32]. Moreover, radioactive ^{90}Sr added to geopolymer in the form of hydroxide was incorporated into amorphous form only partly, being preferentially partitioned to crystalline $SrCO_3$ [33,34]. Thus, the effect of $SrCO_3$ addition to the FA on geopolymer properties is relevant in the context of radioactive strontium immobilization within geopolymers. Barium salts (sulfate and carbonate) can be used for the production of radiation shielding materials. For example, $BaSO_4$-modified FA geopolymer showed promising radiation shielding properties [35]. Cement-based $BaCO_3$-containing composite displayed high potential as a new X-ray shield [36]. Hence, the synthesis of geopolymers based on the (FA + $BaCO_3$) blends may be of significance for protection against X-ray radiation sources.

In this study, strontium and barium carbonates replaced the FA in the amount of 1, 3, 5, 10, 20, and 30 wt.%. Sodium hydroxide solution was used as the alkaline agent and curing was at ambient temperature. Compared to the geopolymers based on the 100% FA, the addition of 1%–10% $SrCO_3$ or $BaCO_3$ to the FA either reduced the strength to some extent or closely matched it. We revealed that the strength growth of geopolymers prepared using mechanically activated mixtures containing 20 and 30% carbonate ($SrCO_3$ or $BaCO_3$) in the initial curing period was lower than that of other studied geopolymers. However, the strength of such geopolymers at the age of 180 d exceeded the strength of geopolymers based on the mixtures containing 0%–10% strontium or barium carbonate. The factors affecting the strength of the synthesized composite geopolymers were discussed.

2. Materials and Methods

2.1. Materials

Class F FA was obtained from a thermal power plant located in Apatity, Murmansk region, Russia. The predominant constituent of the FA was the glass phase, accompanied by crystalline phases, α-quartz, and mullite. A more comprehensive overview of the FA characteristics is given in Ref. [21]. "Pure for analysis" $SrCO_3$ (strontianite) and $BaCO_3$ (witherite) reagents were employed in the formulation of blends. Strontium and barium carbonates were incorporated into the FA at varying concentrations: 1%, 3%, 5%, 10%, 20%, and 30% relative to the total mass of the (FA + carbonate) blend.

2.2. Mechanical Activation

MA of the (FA + carbonates) blends was conducted using an AGO-2 laboratory planetary mill (Novic, Novosibirsk, Russia) under atmospheric conditions at a centrifugal force of 40× *g* for 30–400 s. Steel vials and steel balls with diameters of 7–8 mm were utilized as milling bodies. Further details of MA are reported in Refs. [29–31].

2.3. Preparation of Geopolymers

For the geopolymer synthesis, sodium hydroxide solution (8.3 M) NaOH was used as the alkaline agent. The preparation of geopolymers was performed according to the methodology used in our previous works [29–31]. The milled (FA + carbonate) blends were mixed with NaOH solution to obtain pastes of normal consistency, from which cubes with the size of 1.41 cm × 1.41 cm × 1.41 cm were molded. The mass ratio of Na_2O (present in the NaOH solution) to the milled (FA + carbonate) mixture in the paste was 0.06. The water content was varied to provide the same workability of the pastes. The water/solid ratio (w/s) was determined by considering the amount of water present in the NaOH solution. The compositions of the (FA + $SrCO_3$) and (FA + $BaCO_3$) mixtures used for preparation of the pastes are presented in Tables 1 and 2, respectively. Prepared specimens were cured in a relative humidity of 95% ± 5% at 22 ± 2 °C for 24 h in a closed container. After demolding, the specimens were further cured to testing time in the same conditions used

in the first 24 h. Compressive strength data was obtained from an average of three samples using a hydraulic press PGM-100MG4-A (SKB Stroypribor, Chelyabinsk, Russia).

Table 1. Compositions of (FA + $SrCO_3$) mixtures used for the preparation of pastes.

FA (wt.%)	$SrCO_3$ (wt.%)	w/s Ratio (30 s MA)	w/s Ratio (180 s MA)	w/s Ratio (400 s MA)
100	0	0.23	0.25	0.28
99	1	0.30	0.31	0.31
97	3	0.29	0.31	0.31
95	5	0.29	0.31	0.31
90	10	0.27	0.31	0.30
80	20	0.25	0.25	0.25
70	30	0.24	0.24	0.24

Table 2. Compositions of (FA + $BaCO_3$) mixtures used for the preparation of pastes.

FA (wt.%)	$BaCO_3$ (wt.%)	w/s Ratio (30 s MA)	w/s Ratio (180 s MA)	w/s Ratio (400 s MA)
100	0	0.23	0.25	0.28
99	1	0.30	0.31	0.32
97	3	0.30	0.30	0.30
95	5	0.30	0.30	0.31
90	10	0.30	0.30	0.31
80	20	0.24	0.25	0.26
70	30	0.24	0.24	0.23

2.4. Characterization Methods

The specific surface area of the powders was measured using nitrogen BET method with a Flow-Sorb II 2300 instrument (Micromeritics). Powder X-ray diffraction (XRD) patterns were recorded on a Shimadzu XRD-6000 instrument using Cu–Kα radiation. Scanning was carried out with a step of 0.02° (2 theta) and the dwell time was 1 s. FTIR spectra were recorded with a Nicolet 6700 FTIR spectrometer using potassium bromide tablets. The morphologies of the hydration products were studied using a LEO 420 scanning electron microscope ((Carl Zeiss, Oberkochen, Germany) operated at 20 kV after gold coating on the fractured surface. Thermogravimetric (TG) analysis was performed on a Netzsch STA 449 F3 Jupiter instrument (NETZSCH, Selb, Germany) at a heating rate of 20 °C/min under Ar atmosphere in platinum crucibles.

3. Results and Discussion

3.1. Effect of Mechanical Activation on the (FA + $SrCO_3$) and (FA + $BaCO_3$) Blends

Hardness on Mohs scale of strontianite $SrCO_3$ (3.5) and witherite $BaCO_3$ (3.0–3.5) is close to the hardness of magnesite (4.0–4.5), calcite (3.0) and noticeably less than the hardness of quartz (7.0), mullite (6.3–7.5), and glass phase of fly ash (5.0–6.0) [37–39]. As a result, the intensities of the $SrCO_3$ and $BaCO_3$ peaks in the XRD patterns of the mechanically activated mixtures of FA with these carbonates decreased much more under the influence of MA than those of the quartz and mullite peaks. As a typical example, Figure 1 shows XRD patterns of the (90% FA + 10% MCO_3) (M-Sr, Ba) blends after 30 and 180 s of MA. The decrease in the intensity of $SrCO_3$ and $BaCO_3$ peaks under the influence of MA indicates noticeable structural disturbances and/or a decrease in crystallite size.

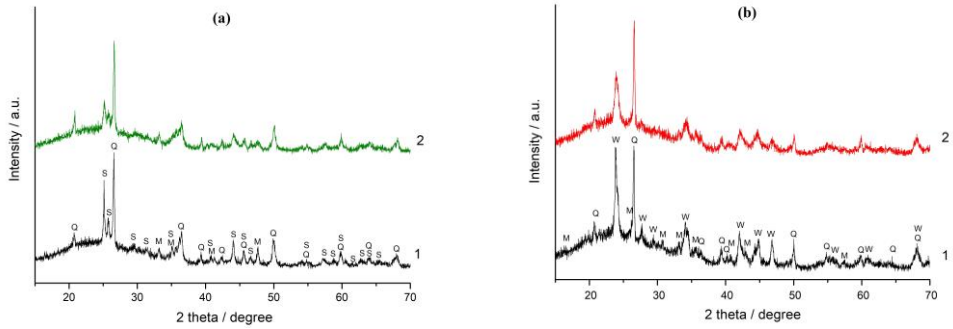

Figure 1. The XRD patterns: 1 (**a**)—the (90% FA + 10% $SrCO_3$) blend milled for 30 s, 2 (**a**)—the same blend milled for 180 s; 1 (**b**)—the (90% FA + 10% $BaCO_3$) blend milled for 30 s, 2 (**b**)—the same blend milled for 180 s. The marked phases are: Q—quartz (ICDD 00-046-1045), M—mullite (ICDD 00-015-0776), S—strontianite $SrCO_3$ (ICDD 00-005-0418), W—witherite $BaCO_3$ (ICDD 00-045-1471).

Milling of the FA blended with strontium and barium carbonates for 30–400 s resulted in a continuous increase in the specific surface area (SSA). At fixed duration of milling the content of carbonate in the blend insignificantly influenced the SSA. The SSA values of (FA + $SrCO_3$) blends milled for 30, 180, and 400 s were 3.8 ± 0.2, 5.8 ± 0.3, and 6.9 ± 0.3 m^2/g, respectively. For the (FA + $BaCO_3$) blends, the corresponding values were 3.5 ± 0.2, 5.4 ± 0.3, and 6.8 ± 0.3 m^2/g, respectively.

3.2. Mechanical Properties

The compressive strength of geopolymers based on the (FA + MCO_3) blends (M-Sr, Ba) cured for 7, 28, and 180 d is shown in Figures 2, 3 and 4, respectively. As in the case of the geopolymers based on the mixtures of FA with calcite, dolomite, and magnesite [29–31], the positive effect of the MA is most evident in the early curing time. For each milling time (30 s, 180 s, and 400 s), average compressive strength values were calculated for a specific curing period (7 d, 28 d, and 180 d) by averaging the strengths of geopolymers based on blends containing 0, 1, 3, 5, 10, 20, and 30% carbonate. After curing for 7 d, the average strength ratios for the geopolymers based on the (FA + $SrCO_3$) blends mechanically activated for 30, 180, and 400 s were 1.0:4.6:7.6, respectively (Figure 2). After 28 and 180 d of curing, the similar proportions were 1.0:2.9:3.3 (Figure 3) and 1.0:1.7:1.6 (Figure 4), respectively. For the geopolymers based on the mechanically activated (FA + $BaCO_3$) blends, the corresponding strength ratios at the age of 7, 28, and 180 d were 1.0:4.1:6.1, 1.0:2.9:3.1, and 1.0:1.7:1.9, respectively.

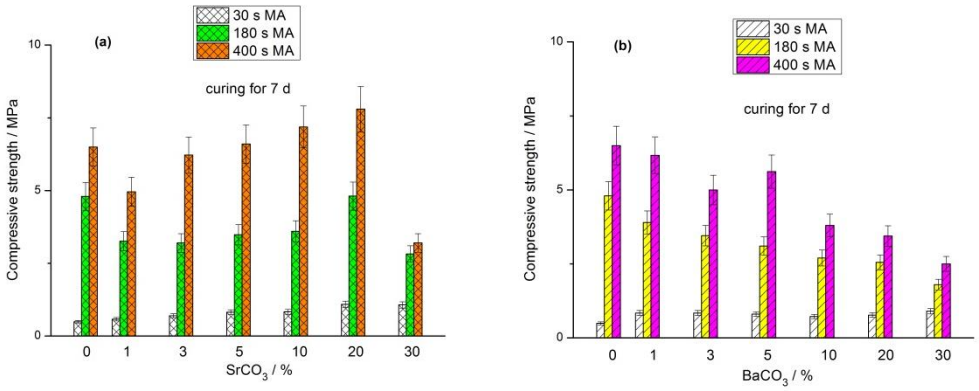

Figure 2. Effect of MA time and carbonate content in the (FA + $SrCO_3$) blend (**a**) and (FA + $BaCO_3$) blend (**b**) on the compressive strength of geopolymers cured for 7 d.

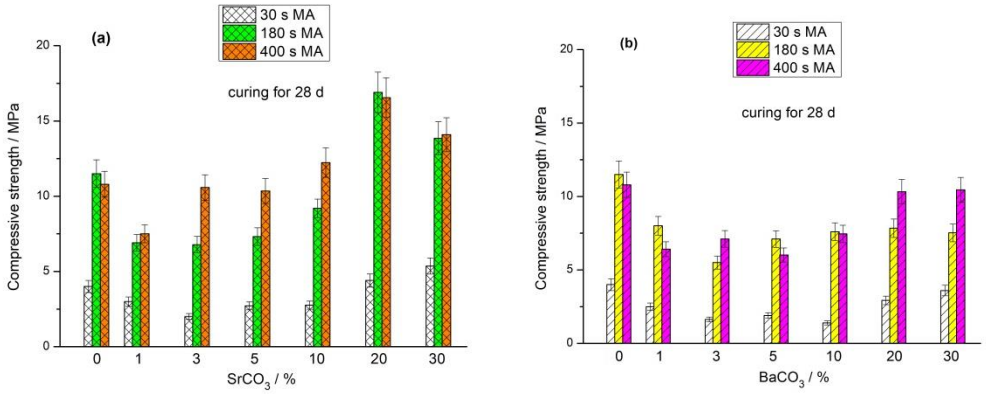

Figure 3. Effect of MA time and carbonate content in the (FA + $SrCO_3$) blend (**a**) and (FA + $BaCO_3$) blend (**b**) on the compressive strength of geopolymers cured for 28 d.

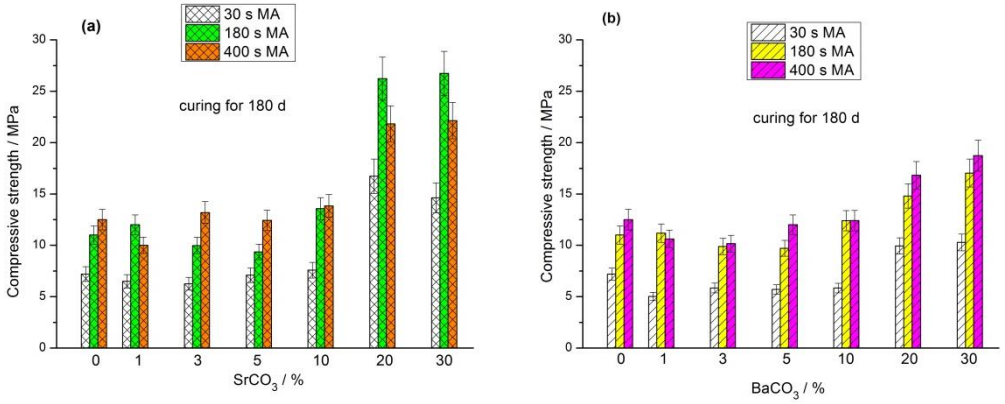

Figure 4. Effect of MA time and carbonate content in the (FA + $SrCO_3$) blend (**a**) and (FA + $BaCO_3$) blend (**b**) on the compressive strength of geopolymers cured for 180 d.

The strength of geopolymers depends on the amount of the main cementitious phase formed, sodium aluminosilicate hydrogel (N-A-S-H gel). As the MA time increased, the amount of fine FA particles in the blends escalated, enhancing the reactivity of FA towards sodium hydroxide solution. Therefore, in the initial curing period (7 d), the rate of N-A-S-H gel formation and, accordingly, the strength of geopolymers based on the blends mechanically activated for 30 s were markedly lower than those of geopolymers synthesized from blends milled for 180 s and 400 s (Figure 2). With increasing curing time (28 and 180 d), after the fine FA particles reacted with the alkaline agent, the strength development rate of geopolymers based on the blends milled for 180 and 400 s decreased compared to that of the geopolymers based on the blends containing initially more coarse particles, i.e., milled for 30 s (Figures 3 and 4).

The strength of all geopolymers based on the (FA + carbonate) blends at the age of 7 d was either less than the corresponding strength of geopolymers based on the 100% FA or within the measurement accuracy was equal to it. The geopolymers synthesized from the (70% FA + 30% $SrCO_3$) and (70% FA + 30% $BaCO_3$) blends exhibited the lowest strength after 7 d of curing (Figure 2). Notably, the strength development of geopolymers derived from the blends containing 20% and 30% carbonate surpassed the strength growth of geopolymers with lower carbonate content as the curing period advanced. After curing for 180 d, the geopolymers with increased content of $SrCO_3$ or $BaCO_3$ (20% and 30% carbonate in the blend) showed the highest performance (Figure 4). This trend was observed largely for the geopolymers containing $SrCO_3$ compared to the geopolymers containing $BaCO_3$. The reasons for this increase are discussed below in Section 3.4. The increased strength of

geopolymers with higher content of Sr and Ba carbonates is consistent with the reduced water content of mixtures used for the preparation of pastes (Tables 1 and 2).

3.3. TG Studies

Figure 5 shows the TG curves of geopolymers synthesized using (90% FA + 10% MCO_3) blends (M-Sr, Ba) milled for 30 s and 180 s at the age of 28 d. For the geopolymers prepared with both carbonates, the mass loss increased with increasing MA time from 30 s to 180 s. With the same MA time, blending the FA with $SrCO_3$ resulted in an increased mass loss compared to blending the FA with $BaCO_3$.

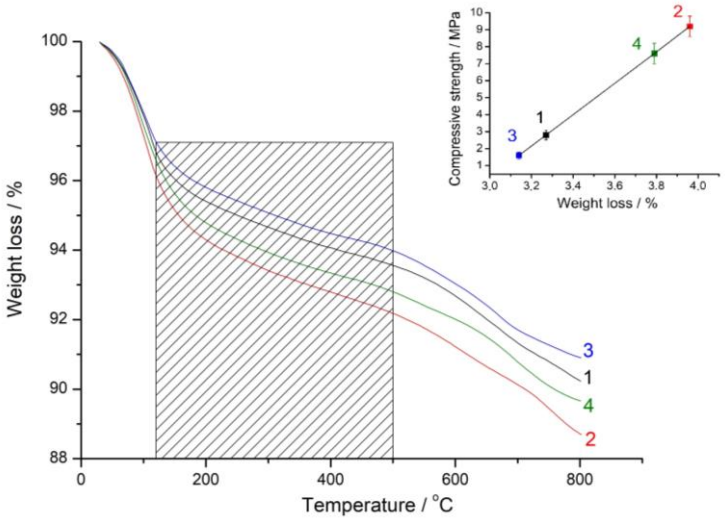

Figure 5. Thermogravimetric (TG) curves of the geopolymers based on the (90% FA + 10% $SrCO_3$) blend milled for 30 s (1), 180 s (2), and based on the (90% FA + 10% $BaCO_3$) blend milled for 30 s (3), 180 s (4). The curing time was 28 d. In the insert, the geopolymer compressive strength vs. the weight loss of the geopolymers in the range of 120–500 °C is shown.

Earlier in the study of geopolymerization of the mechanically activated (FA + calcite) blends, a correlation between the geopolymer strength and the mass loss in the range of 120–500 °C was observed [29]. It is assumed that water tightly bound with N-A-S-H gel is removed in this interval [29,40]. Thus, the mass loss in the shaded area in Figure 5 can serve as a measure of the progress of the geopolymerization reaction. The inset in Figure 5 illustrates the relationship between the strength of geopolymers and the mass loss within the specified temperature range. It can be seen that the geopolymer strength increases in proportion to the mass loss. Simultaneously, in comparison to barium carbonate, strontium carbonate is more effective as an additive to the FA.

3.4. XRD and FT-IR Spectroscopy Analysis

XRD patterns of the (90% FA + 10% $SrCO_3$) and (90% FA + 10% $BaCO_3$) blends mechanically activated for 180 s and geopolymers based on them after 180 d of curing are shown in Figures 6 and 7, respectively. No new crystalline phases were formed as a result of alkaline activation of the blends. The only difference between the XRD patterns of geopolymers and those of the corresponding blends is the increase of amorphous halo in the region of 2 theta angles 25–30°. This indicates the formation of alkaline activation product, amorphous sodium-containing aluminosilicate hydrogel (N-A-S-H gel) [41,42].

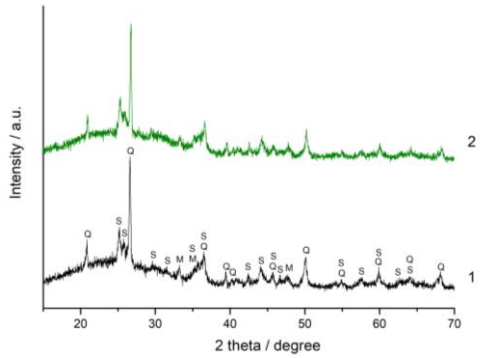

Figure 6. The XRD patterns: 1—the (90% FA + 10% $SrCO_3$) blend milled for 180 s, 2—the geopolymer prepared using the same blend after curing for 180 d. The marked phases are: Q—quartz (ICDD 00-046-1045), M—mullite (ICDD 00-015-0776), S—strontianite $SrCO_3$ (ICDD 00-005-0418).

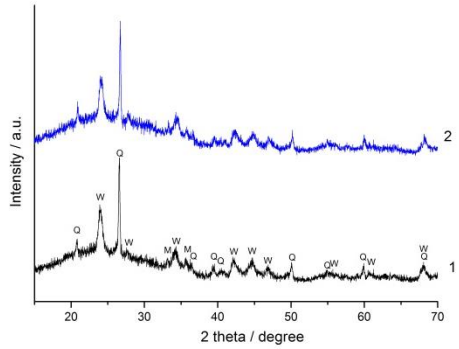

Figure 7. The XRD patterns: 1—the (90% FA + 10% $BaCO_3$) blend milled for 180 s, 2—the geopolymer prepared using the same blend after curing for 180 d. The marked phases are: Q—quartz (ICDD 00-046-1045), M—mullite (ICDD 00-015-0776), W—witherite $BaCO_3$ (ICDD 00-045-1471).

Figures 8 and 9 show the FTIR spectra of the (80% FA + 20% $SrCO_3$) and (80% FA + 20% $BaCO_3$) blends milled for 180 s and the geopolymers based on these mixtures at the ages of 7 d, 28 d, and 180 d. In the spectra of blends, the bands at 1084 cm^{-1} and 461 cm^{-1} correspond to the asymmetric stretching and bending vibrations of the Si-O-T (T-Si, Al) groups, respectively. IR peaks in the region of 820–600 cm^{-1} are due to the presence of quartz and mullite in the FA [42,43].

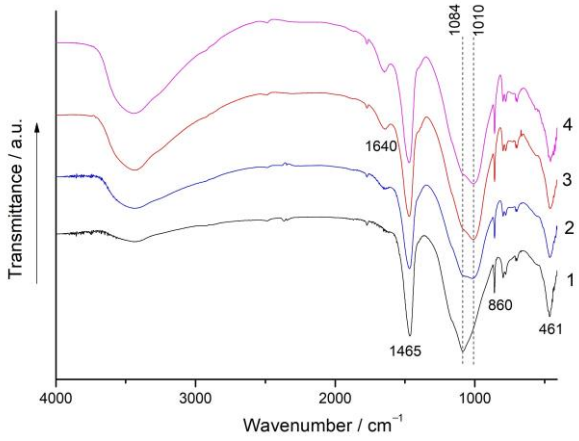

Figure 8. The FTIR spectra: 1—the (80% FA + 20% $SrCO_3$) blend milled for 180 s; 2, 3, and 4—the geopolymers prepared using the same blend after curing for 7 d, 28 d, and 180 d, respectively.

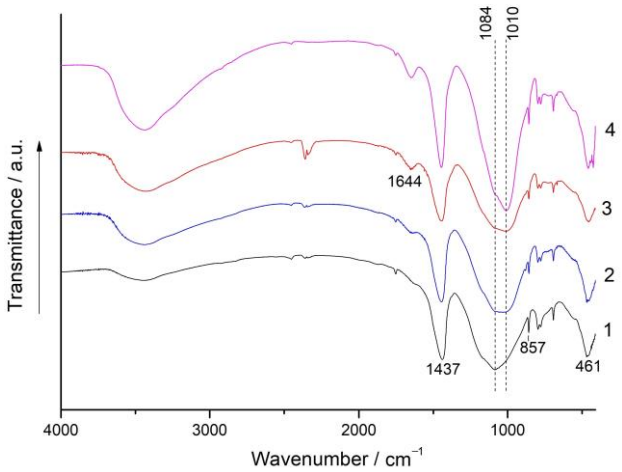

Figure 9. The FTIR spectra: 1—the (80% FA + 20% $BaCO_3$) blend milled for 180 s; 2, 3, and 4—the geopolymers prepared using the same blend after curing for 7 d, 28 d, and 180 d, respectively.

During the geopolymerization of the mixtures, the most noticeable changes in the FTIR spectra occur in the 1100–1000 cm^{-1} region, where an intense absorption band corresponding to the asymmetric stretching vibrations of Si-O-T (T-Si, Al) is located. The maximum of this band shifts to the region of lower wavenumbers as the curing time increases. These changes indicate the formation of a binding product, N-A-S-H gel, and can be attributed to the replacement of Si with Al in silica-oxygen tetrahedrons and a reduction in the degree of polymerization of the aluminosilicate framework of FA [42–46]. For the geopolymers based on both mixtures cured for 180 d, this band is located at 1010 cm^{-1} (Figure 8, curve 4 and Figure 9, curve 4). The gradual increase in the intensity of the broad band of O-H stretching vibrations (3600–3300 cm^{-1}) and H-O-H bending vibrations (1650–1630 cm^{-1}) with curing time indicates an increase in the N-A-S-H gel content [46] in agreement with the development of geopolymer strength (Figures 2–4).

The bands at 1465 and 860 cm^{-1} (Figure 8) correspond to the asymmetric stretching vibrations and symmetric out of plane bending vibrations of the CO_3 group in strontianite, respectively. Similar bands of barium carbonate are located at 1437 and 857 cm^{-1}, respectively (Figure 9) [47]. The shape and position of these bands in the spectra of the geopolymers remain unchanged compared to those in the spectra of the mixtures. In agreement with the XRD data (Figures 6 and 7), this indicates the stability of Sr and Ba carbonates with respect to the alkaline agent.

As mentioned above, the influence of mineral additives on the performance of geopolymers can be explained by the dilution and microfiller effects, as well as the chemical effect. Since $SrCO_3$ and $BaCO_3$ do not interact or very weakly interact with the sodium hydroxide solution according to FTIR spectroscopy (Figures 8 and 9) and XRD data (Figures 6 and 7), the chemical effect is minimized. The strength development of geopolymers based on the blends containing 20 and 30% carbonate at the age of 180 d seems to be due to the effects of dilution and microfiller. The microfiller effect is particularly related to the adhesion of the geopolymer matrix to carbonate particles. This effect requires a certain degree of geopolymerization reaction, i.e., the formation of a sufficient amount of geopolymer gel to ensure a strong contact with the surface of $SrCO_3$ and $BaCO_3$ particles. It is likely that under the synthesis conditions used, the necessary degree of interaction between the FA and the alkaline agent was achieved after 180 d of curing, resulting in an increase in geopolymer strength (Figure 4).

The strength of geopolymers based on the (FA + $SrCO_3$) blends generally exceeds that of corresponding geopolymers containing $BaCO_3$. This trend becomes more pronounced as the carbonate fraction in the blends increases (Figures 2–4). Apparently, this is due to the difference in the chemical properties of Sr and Ba carbonates. $SrCO_3$ (strontianite) and

$BaCO_3$ (witherite) are isostructural, and have the aragonite-type structure. However, the size of Ba^{2+} is larger than that of Sr^{2+}, and the CO_3 group in $BaCO_3$ is more symmetrical and less aplanar than that in $SrCO_3$ [48]. These differences may affect the binding of minerals to the geopolymer gel and, as a consequence, the strength of the geopolymers. Whether this may be due to specific interactions involving binding to carbonate sites or to M^{2+} sites is not clear and requires further investigation. In addition, since $SrCO_3$ and $BaCO_3$ particles act as microaggregates in the composite geopolymer, their hardness should be taken into account [28]. Based on this, the geopolymer containing $SrCO_3$ (Mohs hardness 3.5) would be expected to have a higher compressive strength than a corresponding geopolymer based on the FA blended with $BaCO_3$ (hardness 3.0–3.5), in agreement with the experimental data (Figures 2–4).

3.5. Microstructural Studies

Figure 10 shows representative SEM images of the geopolymers prepared from the (80% FA + 20% $SrCO_3$) blends mechanically activated for 30 s and 180 s at the age of 180 d. Consistent with the strength data (Figure 4), the microstructure of the geopolymer based on the blend milled for 180 s is generally homogeneous and dense (Figure 10c). It is characterized by a lower porosity compared to the geopolymer based on the blend milled for 30 s (Figure 10a). As mentioned above, increasing the MA time from 30 to 180 s resulted in a decrease in the particle size and an increase in the reactivity of the FA towards the alkaline agent. This accelerated the formation of the N-A-S-H gel that fills pores and cracks within the geopolymer structure. In particular, pores may result from the entrainment of air bubbles during mixing (Figure 10c). The appearance of microcracks in Figure 10a,c was most likely due to fracture [49].

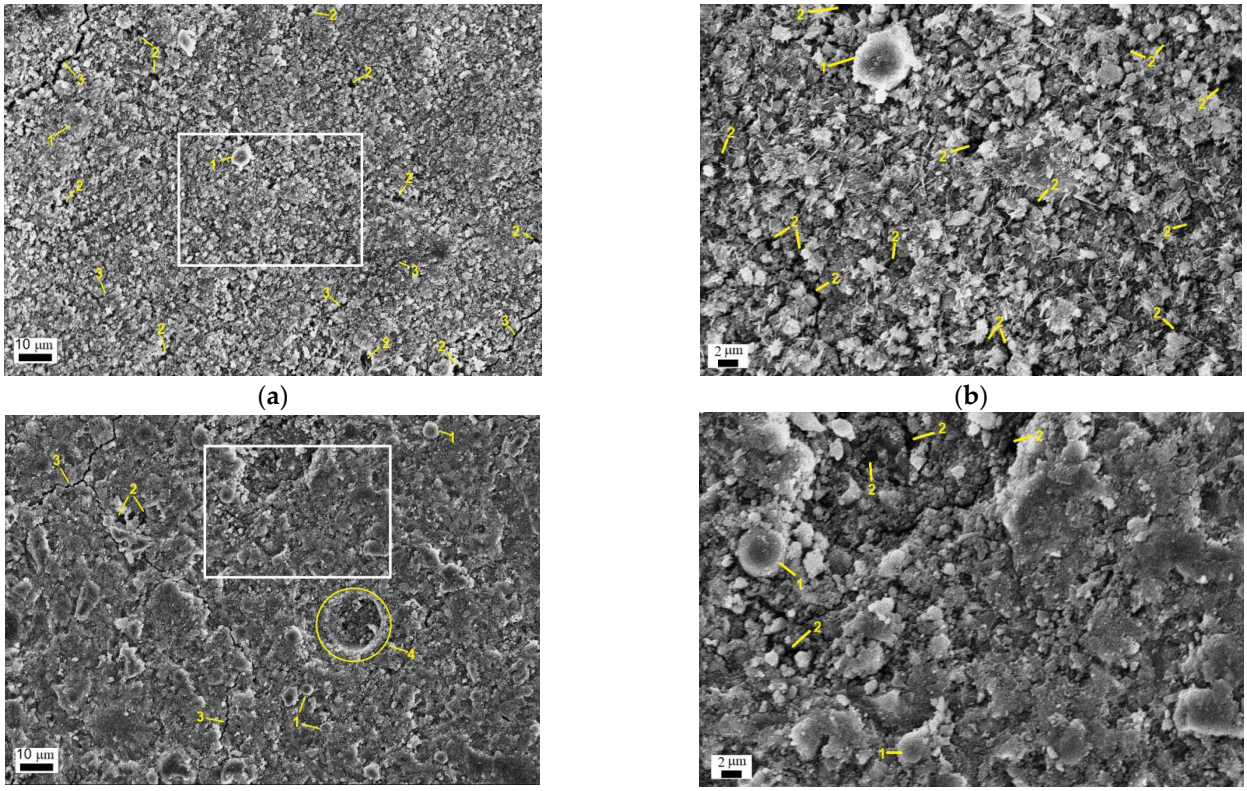

Figure 10. SEM images of the geopolymer synthesized using (80% FA + 20% $SrCO_3$) blend mechanically activated for: (**a**,**b**) 30 s; (**c**,**d**) 180 s. (**b**) and (**d**) are enlarged images shown in the rectangles in (**a**) and (**c**), respectively. The curing time was 180 d. Figure designations: 1—partially reacted FA particles covered with gel; 2—pores; 3—microcracks; 4—cavity left by the trapped air bubble and partially filled with the gel.

A magnified image of the surface of the geopolymer synthesized with the mixture mechanically activated for 30 s shows needle crystals (Figure 10b). Due to the small size of these crystals, it is very difficult to determine their composition by the EDS analysis. Meanwhile, their morphology is typical of crystalline sodium carbonate hydrates formed by the interaction of unreacted alkali with atmospheric carbon dioxide [50,51]. Carbonization of the geopolymer surface apparently occurred during the preparation of the sample for SEM analysis. It should be noted that there are no needle crystals on the surface of the geopolymer prepared from the blend milled for 180 s (Figure 10d). This confirms a more advanced stage of the geopolymerization reaction within this sample, as opposed to the preceding one.

4. Conclusions

The research objects in this work were geopolymers prepared from mechanically activated mixtures of the FA with strontium and barium carbonates. $SrCO_3$ and $BaCO_3$ replaced the FA in the amounts of 1, 3, 5, 10, 20, and 30 wt.%. The MA of the mixtures was carried out in a laboratory planetary mill. Sodium hydroxide solution was used as an alkaline agent and curing was carried out at room temperature. The geopolymers were tested for compressive strength after curing for 7, 28, and 180 d. FTIR spectroscopy, XRD, TGA, and SEM were used to characterize the geopolymers.

The following main conclusions can be drawn based on the results of this study:

1. The intensities of the $SrCO_3$ and $BaCO_3$ peaks in the XRD patterns of the mechanically activated mixtures of FA with these carbonates decreased to a significantly greater extent under the influence of MA compared to the peaks of quartz and mullite. This can be explained by the difference in hardness of the minerals;
2. MA of the (FA + MCO_3) (M-Sr, Ba) blends for 30–400 s resulted in an increase of the specific surface area and an increase in the FA reactivity towards sodium hydroxide solution, in agreement with the TG data and SEM analysis. The geopolymerization reaction product of mechanically activated (FA + $SrCO_3$) and (FA + $BaCO_3$) blends was X-ray amorphous N-A-S-H gel;
3. The positive effect of MA on geopolymers strength was most clearly displayed at early curing times. For 7 d aged geopolymers containing $SrCO_3$, the average strength ratio for the geopolymers based on the blends mechanically activated for 30, 180, and 400 s was 1.0:4.6:7.6, respectively. After curing for 28 and 180 d, the similar ratios were 1.0:2.9:3.3 and 1.0:1.7:1.6, respectively. For the geopolymers based on the mechanically activated (FA + $BaCO_3$) blends, the corresponding strength ratios were 1.0:4.1:6.1, 1.0:2.9:3.1, and 1.0:1.7:1.9 after curing for 7, 28, and 180 d, respectively;
4. Compared to the geopolymer based on the 100% FA, the addition of 1%–30% $SrCO_3$ or $BaCO_3$ to the FA either reduced or had no significant effect on the strength of the 7-d aged geopolymers. As the curing time progressed, the geopolymers synthesized from blends containing 70%–80% FA and 20%–30% $SrCO_3$ or 20%–30% $BaCO_3$ demonstrated superior strength development, exceeding the strength growth of geopolymers containing less carbonates. After 180 d of curing, the geopolymers prepared with (70% FA + 30% carbonate) blends exhibited the highest compressive strength (20–27 MPa);
5. According to the XRD and FTIR spectroscopy data, $SrCO_3$ and $BaCO_3$ were stable with respect to sodium hydroxide solution in the geopolymerization of the blends. The impact of Sr and Ba carbonates addition to the FA on the strength of composite geopolymers can be explained by the dilution and microfiller effects. In particular, the increased strength of geopolymers based on the blends containing 20%–30% carbonate at long curing times (180 d) was most likely due to the adhesion of $SrCO_3$ and $BaCO_3$ particles to the geopolymer matrix under conditions where a sufficient amount of N-A-S-H gel had formed;

6. The strength of geopolymers based on the (FA + $SrCO_3$) blends generally exceeded that of corresponding geopolymers containing barium carbonate, in agreement with the TG data. This was most likely due to the difference in the chemical properties of Sr and Ba carbonates and the ability of the surface of their particles to provide a strong contact with the geopolymer matrix. The enhanced strength exhibited by geopolymers based on the mixtures containing 70%–80% FA and 20%–30% $SrCO_3$ or 20%–30% $BaCO_3$ can be utilized for the immobilization of radioactive strontium and for the formulation of radiation shielding materials.

Author Contributions: Conceptualization, A.M.K. and E.V.K.; methodology, A.M.K., E.V.K., I.A.Z., M.V.C., V.V.S. and E.A.K.; investigation, A.M.K., E.V.K., V.V.S., I.A.Z., M.V.C. and E.A.K.; writing—original draft preparation, A.M.K.; writing—review and editing, A.M.K., E.V.K. and E.A.K.; visualization, M.V.C., V.V.S. and E.A.K. All authors have read and agreed to the published version of the manuscript.

Funding: The reported study was funded by RFBR, project number 20-03-00486.

Data Availability Statement: Data are contained within the article.

Acknowledgments: The study was conducted using the equipment of the Centre for Thermal Analysis and Calorimetry of Saint Petersburg State University Research Park. The authors acknowledge A.G. Ivanova for her help in the preparation of geopolymers.

Conflicts of Interest: The authors declare no conflict of interest.

References

1. Davidovits, J. *Geopolymer Chemistry and Applications*, 5th ed.; Institut Géopolymère: Saint-Quentin, France, 2020; pp. 23–208.
2. Provis, J.L.; Duxson, P.; Kavalerova, E.; Krivenko, P.V.; Pan, Z.; Puertas, F.; van Deventer, J.S.J. Historical aspects and overview. In *Alkali-Activated Materials: State of the Art Report of RILEM TC 224-AAM*; Provis, J.L., van Deventer, J.S.J., Eds.; Springer: Dordrecht, The Netherlands, 2014; pp. 11–58.
3. Tang, Z.; Li, W.; Hu, Y.; Zhou, J.L.; Tam, V.W.Y. Review on designs and properties of multifunctional alkali-activated materials (AAMs). *Constr. Build. Mater*. **2019**, *200*, 474–489. https://doi.org/10.1016/j.conbuildmat.2018.12.157.
4. Luukkonen, T.; Heponiemi, A.; Runtti, H.; Pesonen, J.; Yliniemi, J.; Lassi, U. Application of alkali-activated materials for water and wastewater treatment: A review. *Rev. Environ. Sci. Biol.* **2019**, *18*, 271–297. https://doi.org/10.1007/s11157-019-09494-0.
5. Nodehi, M.; Taghvaee, V.M. Alkali-Activated Materials and Geopolymer: A Review of Common Precursors and Activators Addressing Circular Economy. *Circ. Econ. Sustain.* **2022**, *2*, 165–196. https://doi.org/10.1007/s43615-021-00029-w.
6. Dogan-Saglamtimur, N.; Bilgil, A.; Ertürk, S.; Bozkurt, V.; Süzgeç, E.; Akan, A.G.; Nas, P.; Çetin, H.; Szechynska-Hebda, M.; Hebda, M. Eco-geopolymers: Physico-mechanical features, radiation absorption properties, and mathematical model. *Polymers* **2022**, *14*, 262. https://doi.org/10.3390/polym14020262.
7. Rakhimova, N. Recent Advances in Alternative Cementitious Materials for Nuclear Waste Immobilization: A Review. *Sustainability* **2023**, *15*, 689. https://doi.org/10.3390/su15010689.
8. Phillip, E.; Choo, T.F.; Khairuddin, N.W.A.; Abdel Rahman, R.O. On the Sustainable Utilization of Geopolymers for Safe Management of Radioactive Waste: A Review. *Sustainability* **2023**, *15*, 1117. https://doi.org/10.3390/su15021117.
9. Komljenovic, M.; Tanasijevic, G.; Dzunuzovic, N.; Provis, J. Immobilization of cesium with alkali-activated blast furnace slag. *J. Hazard Mater*. **2020**, *388*, 121765. https://doi.org/10.1016/j.jhazmat.2019.121765.
10. Vandevenne, N.; Iacobescu, R.I.; Pontikes, Y.; Carleer, R.; Thijssen, E.; Gijbels, K.; Schreurs, S.; Schroeyers, W. Incorporating Cs and Sr into blast furnace slag inorganic polymers and their effect on matrix properties. *J. Nucl. Mater*. **2018**, *503*, 1–12. https://doi.org/10.1016/j.jnucmat.2018.02.023.
11. Huang, T.; Song, D.; Yin, L.-X.; Zhang, S.-W.; Liu, L.-F.; Zhou, L. Microwave irradiation assisted sodium hexametaphosphate modification on the alkali-activated blast furnace slag for enhancing immobilization of strontium. *Chemosphere* **2020**, *241*, 125069. https://doi.org/10.1016/j.chemosphere.2019.125069.
12. Tian, Q.; Bai, Y.; Pan, Y.; Chen, C.; Yao, S.; Sasaki, K.; Zhang, H. Application of Geopolymer in Stabilization/Solidification of Hazardous Pollutants: A Review. *Molecules* **2022**, *27*, 4570. https://doi.org/10.3390/molecules27144570.
13. Mohammed, K.S.; Azeez, A.B.; Al Bakri, A.M.M.; Hussin, K.; Rahmat, A.B. The effect of barite content on anti radiation properties of geopolymer fly ash concrete incorporated natural rock ores of hematite. *Int. J. Sci. Res.* **2014**, *3*, 1818–1827.
14. Cantarel, V.; Motooka, T.; Yamagishi, I. *Geopolymers and Their Potential Applications in the Nuclear Waste Management Field—A Bibliographical Study*; JAEA-Review 2017-014; International Atomic Energy Agency (IAEA): Vienna, Austria, 2017.
15. Nurhasmi, H.; Heryanto, H.; Fahri, A.N.; Ilyas, S.; Ansar, A.; Abdullah, B.; Tahir, D. Study on Optical Phonon Vibration and Gamma Ray Shielding Properties of Composite Geopolymer Fly Ash-Metal. *Radiat. Phys. Chem*. **2021**, *180*, 109250. https://doi.org/10.1016/j.radphyschem.2020.109250.

16. Fernandez-Jimenez, A.; Palomo, A. Characterization of fly ashes, potential reactivity as alkaline cements. *Fuel* **2003**, *82*, 2259–2265. https://doi.org/10.1016/S0016-2361(03)00194-7.
17. Duxson, P.; Fernández-Jiménez, A.; Provis, J.L.; Lukey, G.C.; Palomo, A.; van Deventer, J.S.J. Geopolymer technology: The current state of the art. *J. Mater. Sci*. **2007**, *42*, 2917–2933. https://doi.org/10.1007/s10853-006-0637-z.
18. Kumar, S.; Kumar, R. Mechanical activation of fly ash: Effect on reaction, structure and properties of resulting geopolymer. *Ceram. Int.* **2011**, *37*, 533–541. https://doi.org/10.1016/j.ceramint.2010.09.038.
19. Matsuoka, M.; Yokoyama, K.; Okura, K.; Murayama, N.; Ueda, M.; Naito, M. Synthesis of geopolymers from mechanically activated coal fly ash and improvement of their mechanical properties. *Minerals* **2019**, *9*, 791. https://doi.org/10.3390/min9120791.
20. Temuujin, J.; Williams, R.P.; van Riessen, A. Effect of mechanical activation of fly ash on the properties of geopolymer cured at ambient temperature. *J. Mater. Process. Technol.* **2009**, *209*, 5276–5280. https://doi.org/10.1016/j.jmatprotec.2009.03.016.
21. Chu, Y.-S.; Davaabal, B.; Kim, D.-S.; Seo, S.-K.; Kim, Y.; Ruescher, C.; Temuujin, J. Reactivity of fly ashes milled in different milling devices. *Rev. Adv. Mater. Sci.* **2019**, *58*, 179–188. https://doi.org/10.1515/rams-2019-0028.
22. Fernández-Jiménez, A.; Garcia-Lodeiro, I.; Maltseva, O.; Palomo, A. Mechanical-chemical activation of coal fly ashes: An effective way for recycling and make cementitious materials. *Front. Mater.* **2019**, *6*, 51. https://doi.org/10.3389/fmats.2019.00051.
23. Marjanovic, N.; Komljenovic, M.; Bascarevic, Z.; Nikolic, V. Improving reactivity of fly ash and properties of ensuing geopolymers through mechanical activation. *Constr. Build. Mater.* **2014**, *57*, 151–162. https://doi.org/10.1016/j.conbuildmat.2014.01.095.
24. Kumar, R.; Kumar, S.; Alex, T.C.; Singla, R. Mapping of calorimetric response for the geopolymerisation of mechanically activated fly ash. *J. Therm. Anal. Calorim.* **2019**, *136*, 1117–1133. https://doi.org/10.1007/s10973-018-7736-3.
25. Kumar, S.; Kumar, R.; Alex, T.C.; Bandopadhyay, A.; Mehrotra, S.P. Influence of reactivity of fly ash on geopolymerisation. *Adv. Appl. Ceram.* **2007**, *106*, 120–127. https://doi.org/10.1179/174367607X159293.
26. Kato, K.; Xin, Y.; Hitomi, T.; Shirai, T. Surface modification of fly ash by mechano-chemical treatment. *Ceram. Int.* **2019**, *45*, 849–853. https://doi.org/10.1016/j.ceramint.2018.09.254.
27. Rakhimova, N. Calcium and/or magnesium carbonate and carbonate-bearing rocks in the development of alkali-activated cements—A review. *Constr. Build. Mater.* **2022**, *325*, 126742. https://doi.org/10.1016/j.conbuildmat.2022.126742.
28. Yip, C.K.; Provis, J.L.; Lukey, G.C.; van Deventer, J.S. Carbonate mineral addition to metakaolin-based geopolymers. *Cem. Concr. Compos.* **2008**, *30*, 979–985. https://doi.org/10.1016/j.cemconcomp.2008.07.004.
29. Kalinkin, A.M.; Gurevich, B.I.; Myshenkov, M.S.; Chislov, M.V.; Kalinkina, E.V.; Zvereva, I.A.; Cherkezova-Zheleva, Z.; Paneva, D.; Petkova, V. Synthesis of fly ash-based geopolymers: Effect of calcite addition and mechanical activation. *Minerals* **2020**, *10*, 827. https://doi.org/10.3390/min10090827.
30. Kalinkin, A.M.; Gurevich, B.I.; Kalinkina, E.V.; Chislov, M.V.; Zvereva, I.A. Geopolymers based on mechanically activated fly ash blended with dolomite. *Minerals* **2021**, *11*, 700. https://doi.org/10.3390/min1070700.
31. Kalinkin, A.M.; Kalinkina, E.V.; Ivanova, A.G.; Kruglyak, E.A. Effect of magnesite addition and mechanical activation on the synthesis of fly ash-based geopolymers. *Minerals* **2022**, *12*, 1367. https://doi.org/10.3390/min12111367.
32. Provis, J.L.; Walls, P.A.; van Deventer, J.S.J. Geopolymerisation kinetics. 3. Effects of Cs and Sr salts. *Chem. Eng. Sci.* **2008**, *63*, 4480–4489. https://doi.org/10.1016/j.ces.2008.06.008.
33. Jantzen, C.M.; Lee, W.E.; Ojovan, M.I. Radioactive Waste (RAW) Conditioning, Immobilisation, and Encapsulation Processes and Technologies: Overview and Advances. In *Radioactive Waste Management and Contaminated Site Clean-Up: Processes, Technologies and International Experience*; Chapter 6; Woodhead: Cambridge, UK, 2013; pp. 171–272. https://doi.org/10.1533/9780857097446.1.171.
34. Blackford, M.G.; Hanna, J.V.; Pike, K.J.; Vance, E.R.; Perera, D.S. Transmission electron microscopy and nuclear magnetic resonance studies of geopolymers for radioactive waste immobilization. *J. Am. Ceram. Soc.* **2007**, *90*, 1193–1199. https://doi.org/10.1111/j.1551-2916.2007.01532.x.
35. Oglat, A.A.; Shalbi, S.M. An alternative radiation shielding material based on barium-sulphate ($BaSO_4$)-modified fly ash geopolymers. *Gels* **2022**, *8*, 227. https://doi.org/10.3390/gels8040227.
36. Rahmat, R.; Halima, N.; Heryanto, H.; Sesa, E.; Tahir, D. Improvement X-ray radiation shield characteristics of composite cement/Titanium dioxide (TiO_2)/Barium carbonate ($BaCO_3$): Stability crystal structure and chemical bonding. *Radiat. Phys. Chem.* **2023**, *204*, 110634. https://doi.org/10.1016/j.radphyschem.2022.110634.
37. Lide, D.R. (Ed.) *CRC Handbook of Chemistry and Physics*, 89th ed.; CRC Press, Taylor and Francis Group: Boca Raton, FL, USA, 2008; 2736p.
38. Schumann, W. *Handbook of Rocks, Minerals, and Gemstones*; Houghton Mifflin Company: New York, NY, USA, 1993; 380p.
39. Yemelyanova, V.; Dosumova, B.; Dzhatkanbaeva, U.; Shakiyev, E.; Kurokava, H.; Kairbekov, Z.; Muhitova, D.; Shakiyeva, T.; Myltykbaeva, Z. The microspheric catalysts of sodium sulphite low-temperature oxidation by oxygen in water solutions. *Chem. Bull. Kaz. Nat. Univ.* **2013**, *71*, 27–35. https://doi.org/https://doi.org/10.15328/chemb_2013_327-35.
40. Rodríguez, E.D.; Bernal, S.A.; Provis, J.L.; Paya, J.; Monzo, J.M.; Borrachero, M.V. Effect of nanosilica-based activators on the performance of an alkali-activated fly ash binder. *Cem. Concr. Compos.* **2013**, *35*, 1–11. https://doi.org/10.1016/j.cemconcomp.2012.08.025.
41. Kumar, S.; Mucsi, G.; Kristály, F.; Pekker, P. Mechanical activation of fly ash and its influence on micro and nano-structural behaviour of resulting geopolymers. *Adv. Powder Technol.* **2017**, *28*, 805–813. https://doi.org/10.1016/j.apt.2016.11.027.
42. Lee, W.K.W.; van Deventer, J.S.J. Use of infrared spectroscopy to study geopolymerization of heterogeneous amorphous aluminosilicates. *Langmuir* **2003**, *19*, 8726–8734. https://doi.org/10.1021/la026127e.

43. Fernandez-Jimenez, A.; Palomo, A. Mid-infrared spectroscopic studies of alkali activated fly ash structure. *Microporous Mesoporous Mater*. **2005**, *86*, 207–214. https://doi.org/10.1016/j.micromeso.2005.05.057.
44. Rees, C.A.; Provis, J.L.; Lukey, G.C.; van Deventer, J.S.J. In situ ATR-FTIR study of the early stages of fly ash geopolymer gel formation. *Langmuir* **2007**, *23*, 9076–9082. https://doi.org/10.1021/la701185g.
45. Nath, S.K.; Maitra, S.; Mukherjee, S.; Kumar, S. Microstructural and morphological evolution of fly ash based geopolymers. *Constr. Build. Mater.* **2016**, *111*, 758–765. https://doi.org/10.1016/j.conbuildmat.2016.02.106.
46. Rozek, P.; Krol, M.; Mozgawa, W. Spectroscopic studies of fly ash-based geopolymers. *Spectrochim. Acta A Mol. Biomol. Spectrosc*. **2018**, *198*, 283–289. https://doi.org/10.1016/j.saa.2018.03.034.
47. White, W.B. The carbonate minerals. In *The Infrared Spectra of Minerals*; Farmer, W.C., Ed.; Mineralogical Society: London, UK, 1974; pp. 227–284.
48. Antao, S.M.; Hassan, I. The orthorhombic structure of $CaCO_3$, $SrCO_3$, $PbCO_3$ and $BaCO_3$: Linear structure trends. *Can. Mineral.* **2009**, *47*, 1245–1255. https://doi.org/10.3749/canmin.47.5.1245.
49. Rocha, T.d.S.; Dias, D.P.; França, F.C.C.; Guerra, R.R.d.S.; Marques, L.R.d.C.d.O. Metakaolin-based geopolymer mortars with different alkaline activators (Na+ and K+). *Constr. Build. Mater.* **2018**, *178*, 453–461. https://doi.org/10.1016/j.conbuildmat.2018.05.172.
50. Zhang, Z.; Provis, J.L.; Ma, X.; Reid, A.; Wang, H. Efflorescence and subflorescence induced microstructural and mechanical evolution in fly ash-based geopolymers. *Cem. Concr. Compos.* **2018**, *92*, 165–177. https://doi.org/10.1016/j.cemconcomp.2018.06.010.
51. Škvára, F.; Šmilauer, V.; Hlaváček, P.; Kopecký, L.; Cilova, Z. A weak alkali bond in (N, K)–A–S–H gels: Evidence from leaching and modeling. *Ceramics-Silikáty* **2012**, *56*, 374–382.